PHYSICAL REVIEW E **84**, 015202(R) (2011)

Dynamic effects induced by renormalization in anisotropic pattern forming systems

Adrian Keller,[1,2] Matteo Nicoli,[3] Stefan Facsko,[1] and Rodolfo Cuerno[4]

[1]*Institute of Ion Beam Physics and Materials Research, Helmholtz-Zentrum Dresden-Rossendorf, D-01314 Dresden, Germany*

[2]*Interdisciplinary Nanoscience Center, Aarhus University, Ny Munkegade, 8000 Aarhus C, Denmark*

[3]*Physique de la Matière Condensée, École Polytechnique, Centre National de la Recherche Scientifique, 91128 Palaiseau, France*

[4]*Departamento de Matemáticas and Grupo Interdisciplinar de Sistemas Complejos, Universidad Carlos III de Madrid, E-28911 Leganés, Spain*

(Received 3 May 2011; published 18 July 2011)

The dynamics of patterns in large two-dimensional domains remains a challenge in nonequilibrium phenomena. Often it is addressed through mild extensions of one-dimensional equations. We show that full two-dimensional generalizations of the latter can lead to unexpected dynamic behavior. As an example we consider the anisotropic Kuramoto-Sivashinsky equation, which is a generic model of anisotropic pattern forming systems and has been derived in different instances of thin film dynamics. A rotation of a ripple pattern by 90° occurs in the system evolution when nonlinearities are strongly suppressed along one direction. This effect originates in nonlinear parameter renormalization at different rates in the two system dimensions, showing a dynamic interplay between scale invariance and wavelength selection. Potential experimental realizations of this phenomenon are identified.

DOI: 10.1103/PhysRevE.84.015202 PACS number(s): 05.45.−a, 47.54.−r, 68.35.Ct

The self-organized formation of patterns in nonequilibrium systems is a fascinating topic that has been the focus of much attention in the past few decades. Examples range from galaxy formation to sandy dunes to nanostructures [1]. While regular patterns such as stripes and hexagons that are characterized by a single length scale ℓ are well understood when the lateral system size L is comparable to ℓ, their dynamics becomes much more complex in the large domain limit $L \gg \ell$. Indeed, intricate structures ensue, such as spatiotemporal chaos, spiral waves, or quasiperiodic patterns [2]. Another source of complexity derives from dimensionality. While a unified description of one-dimensional (1D) patterns is available through the Ginzburg-Landau equation [1], this is not the case for 2D systems, with strongly anisotropic problems providing particularly challenging cases.

Many systems depending of two space variables are studied within the context of 3D localized structures [3], such as vortices in plasmas [4] or solitary waves in fluids [5,6]. The dynamic equations considered are frequently mild extensions of 1D equations in which only specific terms are turned into 2D operators. This allows one to probe the behavior of a given localized structure when the spatial dimension is increased. In other cases, the equation derives from first principles, as when studying anisotropic surface tension and kinetics in solidification systems [7]. A prototypical model appearing in all these studies is the anisotropic Kuramoto-Sivashinsky (aKS) equation

$$\partial_t h = \nu_x \partial_x^2 h + \nu_y \partial_y^2 h + \frac{\lambda_x}{2}(\partial_x h)^2 + \frac{\lambda_y}{2}(\partial_y h)^2 - \mathcal{K}_x \partial_x^4 h - 2\mathcal{K}_{xy}\partial_x^2\partial_y^2 h - \mathcal{K}_y \partial_y^4 h + \eta. \quad (1)$$

For the sake of definiteness, we will keep in mind a physical picture in which $h(x,y,t)$ is interpreted as the height of a surface above point (x,y) on a reference plane at time t. Indeed, particular instances of Eq. (1) have been derived in various contexts of thin film dynamics such as surface nanopatterning by ion-beam erosion [8], epitaxial growth [9–11], or solidification from a melt [12]. In Eq. (1) the morphological instability leading to pattern formation is implemented by the coefficients $\nu_{x,y}$, at least one of them being negative. Terms with coefficients $\mathcal{K}_j$ provide dissipation at the smallest scales, while the nonlinearities proportional to $\lambda_{x,y}$ stabilize the system. We have incorporated a Gaussian, zero-average uncorrelated noise $\eta(x,y,t)$ as a means to explore the aKS equation in a large domain. Indeed, for $L \gg \ell$, the deterministic Kuramoto-Sivashinsky (KS) equation is well known to display spatiotemporal chaos and a steady state with strong height fluctuations [13,14]. Introduction of noise helps to elucidate these for times after the onset of the morphological instability [15–17], while it is not essential for the occurrence of the morphological transition we are studying in this paper.

Regarding Eq. (1) as a model of 3D localized structures, e.g., the description of solitary fluid waves moving down an inclined plane, corresponds to $\nu_y = \lambda_y = 0$, $\mathcal{K}_x = \mathcal{K}_y = \mathcal{K}_{xy}$ [6,18], while in the solidification system $\nu_y = -\nu_x$, $\lambda_y = \mathcal{K}_y = \mathcal{K}_{xy} = 0$ [7]. Thus Eq. (1) is tailored to preserving the quasi-one-dimensional features of specific solutions. In this work we show that small deviations from fine-tuned conditions such as the latter are able to induce dynamic effects in the system that unavoidably require a full two-dimensional description. Specifically, a rippled pattern appearing at short times along one of the system directions rotates by 90° during the evolution, leading at longer times to ripples oriented in the perpendicular direction. This dynamic transition occurs as a result of the different rates at which fluctuations renormalize due to the inhomogeneous strengths of nonlinear effects along the two space dimensions.

We start by exploring numerically the behavior of Eq. (1). It is convenient to first bring it to a dimensionless form. As the properties to be studied are not conditioned by the anisotropy of the dissipative terms, we will restrict ourselves to the case in which $\mathcal{K}_x = \mathcal{K}_y = \mathcal{K}_{xy} \equiv \mathcal{K}$. Then, defining rescaled coordinates $t' = -(|\nu_x|\nu_x/\mathcal{K})t$, $\mathbf{x}' = (|\nu_x|/\mathcal{K})^{1/2}\mathbf{x}$, and $h' = -(\lambda_x/2\nu_x)h$ leads to

$$\partial_t h = -\partial_x^2 h - a_\nu \partial_y^2 h + (\partial_x h)^2 + a_\lambda (\partial_y h)^2 - \nabla^4 h + \xi, \quad (2)$$

 ©2011 American Physical Society

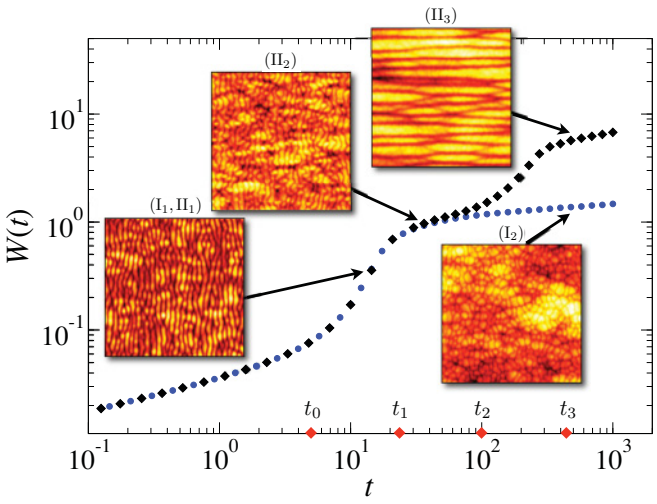

FIG. 1. (Color online) Surface roughness vs time for conditions I (circles) and II (diamonds). Simulations of Eq. (2) are performed with $a_\nu = 0.1$, $D = 10^{-2}$, $\Delta t = 5 \times 10^{-3}$, $L = 512$, $\Delta x = 1$, and $a_\lambda = 0.5$ (I) and 0.025 (II). $W(t)$ is averaged over 100 noise realizations. Top views of the surface morphology (size $L/2$; see [22] for larger sizes) are shown for conditions I and II at times as indicated by arrows. Times t_j in the main text appear as diamonds on the horizontal axis. All units are arbitrary.

where primes are dropped, ξ is a noise term with a rescaled variance, and the ratios $a_\nu = \nu_y/\nu_x$ and $a_\lambda = \lambda_y/\lambda_x$ control the linear and nonlinear anisotropies, respectively. We perform numerical simulations of Eq. (2) for flat initial conditions by using both a finite difference scheme with periodic boundary conditions [19] and, alternatively, a pseudospectral scheme [20,21].

Figure 1 shows the time evolution of the surface roughness $W^2(t) = \langle (1/L^2) \sum_{\mathbf{r}} [h_{\mathbf{r}}(t) - \bar{h}(t)]^2 \rangle$, where angular brackets denote the average over noise realizations and an overbar denotes the space average. Two different parameter conditions are considered for $a_\nu < 1$ [22]. In the first one (I), the nonlinear couplings are comparable in two directions x and y ($a_\lambda = 0.5$), while the second one (II) is representative of conditions in which λ_y is strongly suppressed ($0 < a_\lambda \lesssim 0.1$). The values of time at which $W(t)$ changes behavior significantly are marked by showing the corresponding surface morphologies. For both conditions $a_\nu < 1$ induces a linear instability leading to the formation of a ripple structure with crests oriented parallel to the y axis. This takes place at time t_0 in Fig. 1, at which $W(t)$ grows exponentially. The corresponding morphologies are statistically indistinguishable for both conditions, so a single common snapshot (I_1,II_1) is shown in Fig. 1. For later times this regime is followed by nonlinear stabilization inducing at time t_1 a slower, power-law growth rate for $W(t)$. Morphologically, this type of growth is characterized by a progressive blurring of the early time pattern (morphology I_2) and the dominance of height fluctuations associated with kinetic roughening [13,23]. For condition II noise effects also dominate for time $t_1 < t < t_2$ (morphology II_2). At time $t = t_2$ there is a second rapid increase in $W(t)$ that morphologically corresponds to the formation of a new ripple structure, but now with crests parallel to the x axis. The wavelength of this new pattern is larger than that of the initial one; see morphology II_3. Again, nonlinear effects stabilize growth in amplitude for times $t > t_3$, thus $W(t)$ displays kinetic roughening properties similar to those occurring for condition I at long times [23].

In the simulations a_λ is always positive, thus the known cancellation modes of the aKS equation [11] are not solutions of Eq. (2). The dynamic behavior seen so far can be interpreted by using the results for the noisy 1D KS equation. Thus, as already argued for by Yakhot [24] in the deterministic limit, the noisy KS (nKS) equation is known to undergo a renormalization process through which the negative coefficient of the second-order linear term becomes effectively positive (and therefore stable) at sufficiently large space and time scales [16,25]. This effect is induced by the nonlinearity and allows for its eventual control of the scaling behavior at the stationary state, which is in the Kardar-Parisi-Zhang (KPZ) universality class [13]. Analogous behavior has recently been shown to occur in the 2D isotropic nKS case [17]. Morphologically, the linear pattern forming instability occurring at short times is followed by a disordered height morphology showing kinetic roughening properties of the KPZ class asymptotically.

In the case of the aKS equation (2) with small a_λ, this renormalization can be expected in the x direction, resulting in a stabilizing value $\nu_x^* > 0$. In the y direction, however, the nonlinearity is so weak that the transition to the nonlinear regime is strongly delayed. Therefore, at times $t \simeq t_2$ when ν_x^* has already renormalized to a positive value, the corresponding ν_y^* coefficient has not yet and remains negative. Then a new linear instability in the y direction causes the formation of a ripple pattern that appears rotated by 90° with respect to the early time pattern. These ripples grow exponentially in time until the values of the slopes along the y direction become so large that the corresponding nonlinearity in Eq. (2) takes over and the new ripple amplitude is stabilized. One can estimate the value of the time t_3 at which this happens by equating the contributions of the linear and nonlinear parts of the equation, with the result [23]

$$t_3 \propto a_\nu^{-1} \ln(a_\nu/a_\lambda). \tag{3}$$

The linear wavelength of the rotated pattern should be given by $\ell_y = 2\pi(2/a_\nu)^{1/2}$.

Quantitative comparisons between the simulated and the analytical dependence of t_3 on a_λ and a_ν are shown in Figs. 2(a) and 2(b), respectively. Also, ℓ_y is shown in the inset of Fig. 2(b) as a function of a_ν as obtained from simulations and as calculated from the linear approximation. In all cases, values from simulations agree well with analytical estimates, supporting our interpretation of the dynamic morphological transition within the framework of parameter renormalization.

Further progress is possible by studying Eq. (1) within a one-loop dynamic renormalization group (DRG) approach. After its application to fluctuating hydrodynamics [26], this method has recently shown a large explanatory power in related contexts, such as multiscale descriptions of fluctuating interfaces [27] or morphological instabilities mediated by nonlocal interactions [28]. Following the standard approach [26], we arrive at the following RG parameter flow [22]:

$$\frac{dr}{dl} = r\left(\frac{\Sigma_{\nu_y}}{\nu_y} - \frac{\Sigma_{\nu_x}}{r\nu_y}\right), \quad \frac{dg}{dl} = g\left(3\frac{\Sigma_{\nu_y}}{\nu_y} + \frac{\Phi}{D}\right), \tag{4}$$

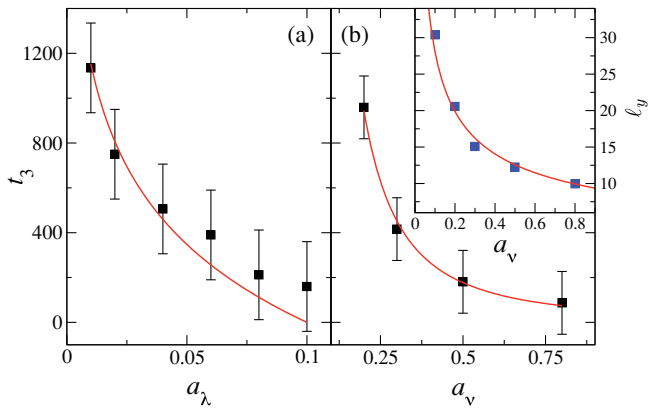

FIG. 2. (Color online) Transition time t_3 vs (a) a_λ for $a_\nu = 0.1$ and (b) a_ν for $a_\lambda = 10^{-3}$. Solid lines represent fits according to Eq. (3) with a prefactor as a fitting parameter. The inset in (b) shows the wavelength ℓ_y of the rotated pattern as a function of a_ν, as determined from the simulations for $a_\lambda = 10^{-3}$ (blue squares; error bars are smaller than the symbol size) and calculated within a linear approximation (red line). All units are arbitrary.

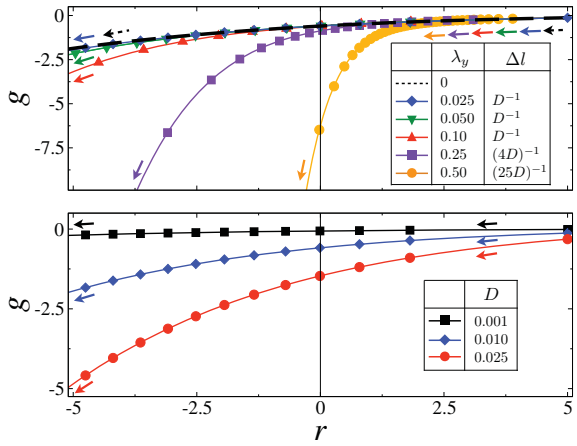

FIG. 3. (Color online) DRG flow of the couplings r and g. The numerical integration of Eqs. (4) has been carried out using $\nu_x = -1$, $\nu_y = -0.1$, $\lambda_x = 1$, $\mathcal{K}_x = \mathcal{K}_y = \mathcal{K}_{xy} = 1$, and values of λ_y and D as shown in the legends. The top panel is for fixed $D = 10^{-2}$ and changing λ_y. Note that g renormalizes even for $\lambda_y = 0$. Markers display values of (r,g) separated by Δl as shown in the legend, while arrows show the direction of the RG flow. The bottom panel is for fixed $\lambda_y = 0.025$ and different values of D with $\Delta l = 1/D$. All units are arbitrary.

where a coarse graining of the height and noise fields has been performed in a fast mode shell in wave-vector space $\mathbf{k}$ with $k \in [\Lambda(1-dl),\Lambda]$, where $\Lambda = 1$ is a lattice cutoff. Here $r = \nu_x/\nu_y$ and $g = \lambda_x^2 D/\pi^2\nu_y^3$, with D being the noise variance. Equations (4) generalize the DRG analysis of the anisotropic KPZ equation in Ref. [10]. The functions Σ_{ν_j} originate from propagator renormalization, whereas Φ arises in noise variance renormalization [22]. The flow Eqs. (4) has been derived within the further assumption that, as expected [16,25], the parameters $\mathcal{K}_j$ become enslaved [29] to the slower parameter ν_y in Eq. (1). In Fig. 3 we show results from a numerical integration of Eqs. (4). Starting from conditions for which ν_x and ν_y are both negative, the parameter r is seen to cross the zero value, which means that, at the corresponding scale l, $\nu_x(l)$ has become positive and stabilizing while $\nu_y(l)$ remains negative. After further coarse graining, g decreases to $-\infty$, signaling renormalization of ν_y toward positive values, which in turn requires crossing $\nu_y = 0$ at the appropriate (large) scale. Note that the larger λ_y is, the faster renormalization of g takes place, as denoted by the relative spacing among points evaluated at equally spaced positions $n\Delta l$ along the corresponding flow trajectories. Once both ν_j coefficients have renormalized to positive values, by analogy with the 1D and the isotropic 2D cases for the nKS equation, one expects the system to enter the anisotropic KPZ regime [10]. Within this picture, a stationary state is expected at long times, which shows kinetic roughening. As in the nKS case [15,16], this state is more efficiently reached when the noise variance is larger, as seen in the bottom panel of Fig. 3, where g renormalizes faster for increasing D values. Indeed, the slow growth of $W(t)$ at long times for condition II in Fig. 1 signals the stabilization of the second ripple structure by nonlinear effects. Note that this is also the case for condition I for which no second ripple structure exists. Thus bare values of the nonlinearities that are comparable to each other (condition I) lead to faster renormalization of $\nu_{x,y}$ to stable positive values and to a rough, disordered stationary state, as implied by the top panel in Fig. 3.

The present dynamic morphological transition induced by renormalization effects can be intuitively understood by an argument that employs knowledge of a particular solution of Eq. (1) for the case in which $\lambda_y = 0$. In this extreme limit one can assume [11] that $h(x,y,t) = H(y,t)$ does not depend explicitly on x, thus $\partial_x^n H = 0$, even for nonzero ν_x and λ_x. Substituting this ansatz into Eq. (1), we get $\partial_t H = \nu_y\partial_y^2 H - \mathcal{K}_y\partial_y^4 H + \eta$, which is a linearized 1D nKS equation for H because $\nu_y < 0$. Therefore, $H(y,t)$ is a ripple structure with crests along the x direction. Moreover, linear stability analysis leads to a dependence of the wavelength of this ripple structure precisely as determined for ℓ_y in Fig. 2 once rescaled coordinates are employed as in Eq. (2). Note, however, that $H(y,t)$ is not a solution of Eq. (1) for conditions II. Still, starting from a flat initial surface, the term $\mathcal{N}_y = \lambda_y(\partial_y h)^2$ stays negligible until $t \simeq t_2$, at which point the full solution $h(x,y,t) \approx H(y,t)$. Since the latter solution is itself morphologically unstable, large values of $\partial_y h \approx \partial_y H$ build up that make the term $\mathcal{N}_y$ no longer negligible. This introduces significant differences between h and H after $t > t_3$. A limitation of this argument is its neglect of dynamics up to $t = t_2$. At earlier times, a ripple structure exists in the perpendicular direction, for which it is y derivatives, rather than x derivatives, that are small (see, e.g., morphology I_1,II_1 in Fig. 1). For the solution $H(y,t)$ to become dynamically relevant, the initial ripple structure needs to be washed out by fluctuations and nonlinearity as in condition I, which requires the renormalization process discussed above.

A dynamic transition reminiscent of the one considered here has been observed experimentally in high-temperature surface nanopatterning by ion-beam sputtering (IBS) of Si(111) surfaces [30,31]. Specifically, at low fluence (equivalent to time for the fixed flux conditions employed), a ripple pattern with crests perpendicular to the direction of the incident ion beam formed on the surface, with a wavelength $\ell_x \simeq 300$–

500 nm. At intermediate fluence, however, a different ripple pattern rotated by 90° overlayed the initial one, resulting in a pattern of dotlike features. At even higher fluence, the initial pattern vanished and only the rotated pattern, with a significantly larger wavelength $\ell_y > 500$ nm, remained. The experimentally observed rotation of the ripple pattern by 90° does not agree with the predicted angle for cancellation modes, which under these experimental conditions is expected to be 25° [30]. Hence the observed ripple rotation is not related to the appearance of cancellation modes and must be of a different origin. Given the striking similarities to the transition studied in our work, a strong nonlinear anisotropy with $a_\lambda \ll 1$ can be assumed for the experimental system. Transient morphologies of two-dimensional features similar to those observed in Refs. [30,31] can also be achieved in the simulations of the aKS equation by tuning the coefficients a_ν and a_λ in such a way that the growth of the rotated ripples sets in before the initial pattern has fully vanished [22]. Although the physical picture leading to the aKS equation as a physical model for IBS has recently been contested (see a review in Ref. [32]), the high-temperature condition employed in these experiments can be expected to enhance surface transport. In such a case, an aKS-type equation holds with modified coefficients [32], which may, moreover, account for the lack of cancellation modes in the experiments as compared with theoretical estimates derived from Refs. [8,30,31].

In summary, we have obtained a dynamic transition in the evolution of anisotropic patterns that illustrates the rich phenomena that occur when taking into account the full anisotropy in this class of nonequilibrium systems. The transition merges two apparently opposed phenomena, such as the selection of a typical wavelength and strong morphological fluctuations leading to renormalization and scale invariance. Actually, the dominance of the latter at intermediate times seem to be a requirement for the development of the pattern that later emerges. A dynamic role seems to be played also by approximate solutions of the equation, such as cancellation modes. This suggests an interest in exploring such types of solutions in other anisotropic, pattern forming systems. In its stabilized form, the isotropic KS equation has been shown to provide a generic model for parity-symmetric systems featuring a bifurcation with a vanishing wave number [33]. Thus we expect the phenomenology of the aKS equation to apply quite generically. In particular, the transition that we have discussed may offer an explanation for the recently observed ripple rotation in high-temperature IBS nanopatterning experiments on Si surfaces [30]. Further theoretical and experimental work is needed in order to elucidate the degree to which this is actually the case and the appearance of related phenomena in other pattern forming systems.

A.K. acknowledges financial support from the Alexander von Humboldt Foundation. M.N. and R.C. acknowledge partial support by Ministerio de Ciencia e Innovación (Spain) Grant No. FIS2009-12964-C05-01.

[1] M. Cross and H. Greenside, *Pattern Formation and Dynamics in Nonequilibrium Systems* (Cambridge University Press, Cambridge, England, 2009).
[2] M. C. Cross and P. C. Hohenberg, Rev. Mod. Phys. **65**, 851 (1993).
[3] S. Toh, H. Iwasaki, and T. Kawahara, Phys. Rev. A **40**, 5472 (1989).
[4] E. A. Kuznetsov, A. M. Rubenchik, and V. E. Zakharov, Phys. Rep. **142**, 103 (1986).
[5] H.-C. Chang and E. A. Demekhin, *Complex Wave Dynamics on Thin Films* (Elsevier, Amsterdam, 2002).
[6] E. A. Demekhin, E. N. Kalaidin, S. Kalliadasis, and S. Y. Vlaskin, Phys. Rev. E **82**, 036322 (2010).
[7] S. H. Davis, *Theory of Solidification* (Cambridge University Press, Cambridge, England, 2001).
[8] R. Cuerno and A.-L. Barabási, Phys. Rev. Lett. **74**, 4746 (1995).
[9] J. Villain, J. Phys. I **1**, 19 (1991).
[10] D. E. Wolf, Phys. Rev. Lett. **67**, 1783 (1991).
[11] M. Rost and J. Krug, Phys. Rev. Lett. **75**, 3894 (1995).
[12] A. A. Golovin and S. H. Davis, Physica D **116**, 363 (1998).
[13] J. Krug, Adv. Phys. **46**, 139 (1997).
[14] M. Pradas, D. Tseluiko, S. Kalliadasis, D. T. Papageorgiou, and G. A. Pavliotis, Phys. Rev. Lett. **106**, 060602 (2011).
[15] R. Cuerno, H. A. Makse, S. Tomassone, S. T. Harrington, and H. E. Stanley, Phys. Rev. Lett. **75**, 4464 (1995).
[16] K. Ueno, H. Sakaguchi, and M. Okamura, Phys. Rev. E **71**, 046138 (2005).
[17] M. Nicoli, E. Vivo, and R. Cuerno, Phys. Rev. E **82**, 045202 (2010).
[18] V. I. Petviashvili, Physica D **3**, 329 (1981).
[19] A. Keller, S. Facsko, and R. Cuerno, in *Computational Nanotechnology: Modeling and Applications with Matlab*, edited by S. M. Musa (CRC, Boca Raton, FL, 2011).
[20] L. Giada, A. Giacometti, and M. Rossi, Phys. Rev. E **65**, 036134 (2002).
[21] L. Giada, A. Giacometti, and M. Rossi, Phys. Rev. E **66**, 019902(E) (2002).
[22] See Supplemental Material at http://link.aps.org/supplemental/10.1103/PhysRevE.84.015202 for movies of the dynamics for conditions I, II, etc., and details on the RG flow equations (4).
[23] S. Park, B. Kahng, H. Jeong, and A.-L. Barabási, Phys. Rev. Lett. **83**, 3486 (1999).
[24] V. Yakhot, Phys. Rev. A **24**, 642 (1981).
[25] R. Cuerno and K. B. Lauritsen, Phys. Rev. E **52**, 4853 (1995).
[26] W. D. McComb, *The Physics of Fluid Turbulence* (Oxford University Press, New York, 1991).
[27] C. A. Haselwandter and D. D. Vvedensky, Phys. Rev. Lett. **98**, 046102 (2007).
[28] M. Nicoli, R. Cuerno, and M. Castro, Phys. Rev. Lett. **102**, 256102 (2009).
[29] H. Haken, *Synergetics: Introduction and Advanced Topics* (Springer, New York, 2004).
[30] A.-D. Brown, J. Erlebacher, W.-L. Chan, and E. Chason, Phys. Rev. Lett. **95**, 056101 (2005).
[31] A.-D. Brown and J. Erlebacher, Phys. Rev. B **72**, 075350 (2005).
[32] R. Cuerno, M. Castro, J. Muñoz-García, R. Gago, and L. Vázquez, Nucl. Instrum. Methods Phys. Res. B **269**, 894 (2011).
[33] C. Misbah and A. Valance, Phys. Rev. E **49**, 166 (1994).